Chapter 3

Method

In this chapter, we discussed the method that is used in various experiments. The detailed methods of sample preparation and specific instrumentation are included in each chapter.

3.1 Confocal Microscope

The main purpose of a confocal microscope is to generate a point light source by reducing the out-of-focus light using pinhole apertures on both the illumination and detection sides within the same conjugate image plane, rendering them "confocal." first discovered by Minsky.[137] The fundamental premise of confocal microscopy is that the illumination and detection optics converge on the same diffraction-limited point, which is travelled over the sample to construct the high-resolution image. A confocal microscope consists of a) a light source (diode/lasers/ solid-state lasers), b) a detector (PMT), c) an acousto-optic tunable filter (AOTF) for tuning the laser and d) other filters (dichroic or bandpass depending upon the wavelength of fluorophore), e) fast scanning mirror f) Objective lens (Figure 3.1). The pinhole plays a big role here; depending upon the confocal aperture (C.A) of the pinhole, one can play with intensity and resolution; with increasing the C.A., the intensity will increase but at the expense of the resolution of the image. The lateral and axial resolution are ~0.2 μm and ~0.6 μm, though it may depend upon the setup. The formulas employed to ascertain lateral and axial resolution are as follows, where NA signifies the numerical aperture of the objective:[138]

$$R_{lateral} = \frac{0.4\lambda}{NA} \quad (3.1)$$

$$R_{axial} = \frac{1.4\times\lambda\times\eta}{(NA)^2} \quad (3.2)$$

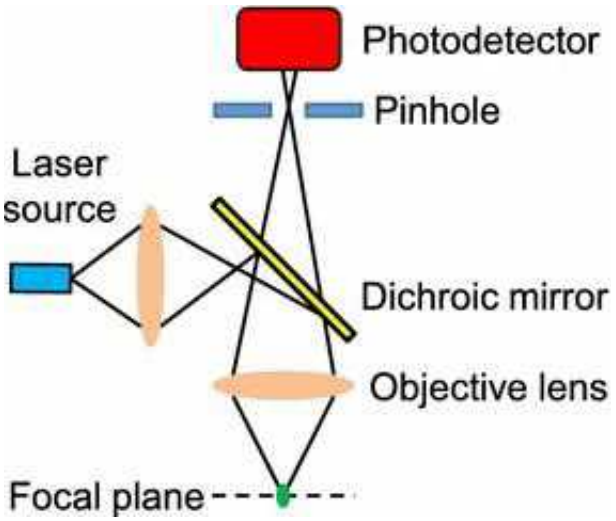


Figure 3.1 The simplest diagram of the Confocal Microscope. The figure is reproduced with from D. Fukuda (2018).[139]

3.2 Solvation Dynamics

3.2.1 Basic Principle

Solvation dynamics denote the response of solvent dipoles by surrounding instantaneous dipole or an electron/proton that is abruptly introduced into a polar liquid. To comprehend the significance and extent of solvation dynamics, we must first conceptualize the physical nature of the dynamic process occurring for a solute molecule in a polar solvent.[140-141] First, a probe/solute dipole is induced at time zero time, initiated by a short laser pulse, which instantly gives an electric field in the solvent molecules. With increasing time, the solvent molecules started to rearrange themselves around the dipole of solute molecules; hence, the system's energy decreased.

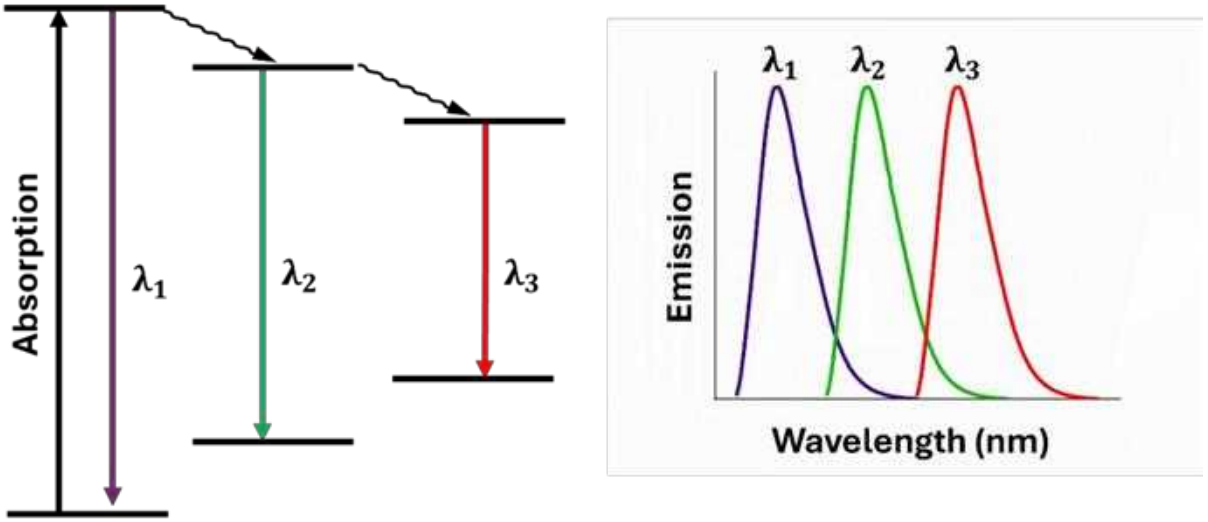


Figure 3.2 Fluorescence stock shift, which is dependent on solvation and time.

3.2.2 Time-Resolved Emission Spectrum Calculation

To investigate the solvation stabilization of a probe inside an environment, several fluorescence transients are recorded at various wavelengths throughout the probe's emission spectrum. As per the literature, the blue end exhibits decay and the red end is expected to demonstrate a rise in the transients in the fluorescence spectra (Figure 3.2). The TRES is generated according to the methodology outlined by Fleming and Maroncelli.[142] The analysis relies on the fluorescence decay parameters across several wavelengths and the SSE. The time and wavelength-dependent intensity $I(\lambda, t)$ can be defined as $I(\lambda, t) = A(\lambda)B(t)$ where $B(t)$, which is derived from the optimal fits to the temporal decay. $A(\lambda)$ can be derived from the SSI, $ISS(\lambda)$, as follows:[143]

$$I_{ss}(\lambda) = \int_0^\infty I(\lambda, t)dt = A(\lambda) \int_0^\infty B(t)dt \quad (3.3)$$

Where, $B(t) = \sum_i a_i e^{\left(-\frac{t}{\tau_i}\right)}$

So, $A(\lambda) = \frac{I_{SS}(\lambda)}{\int_0^\infty B(t)dt} = \frac{I_{SS}(\lambda)}{\sum_i a_i \tau_i}$ (3.4)

In the equation mentioned above (equation 3.3), a_i and τ_i represent the amplitudes and decay constants of the temporal decay. $I_{SS}(\lambda)$ represents the steady-state intensity, which may be derived from the steady-state emission spectra. Given that all parameters in equation 3.3 are

known, the value of A (λ) can be calculated. Ultimately, by substituting the values of A (λ) and B (t) into equation 3.3, one obtains the intensity dependent on time and wavelength.

$$I(\lambda, t) = A(\lambda)B(t) = \frac{I_{SS}(\lambda)}{\sum_i a_i \tau_i} \sum_i a_i \, e^{\left(-\frac{t}{\tau_i}\right)} \quad (3.5)$$

Upon acquiring the time dependence of the intensity, it becomes very simple to generate the TRES at various time intervals by computing I(λ,t) for distinct λ and t. The emission maxima at each time ν(t) are derived from the optimal fitting of the TRES.

The decay of the solvent correlation function C(t) is defined as follows:[142]

$$C(t) = \frac{\nu(t) - \nu(\infty)}{\nu(0) - \nu(\infty)} \quad (3.6)$$

ν(0), ν(t), and ν(∞) represent the peak frequencies at times 0, t, and ∞, respectively. The value of ν(∞) is determined by fitting ν(t) to time (t) using the equation 3.6 $\nu(t)=\nu(\infty) + [\nu(0)-\nu(\infty)] \{\Sigma a_i \exp(-t/\tau_i)\}$.

It should be noteworthy that a significant fraction of solvation dynamics occurs on an ultrafast timescale and remains undetected even with a femtosecond setup. The quantity of solvation missed in a setup can be readily determined using the Fee and Maroncelli approach.[142] When the solute probe is excited at its absorption maximum, the difference between the emission at time zero $\nu_{em}^{p}(0)$ and the absorption frequency (ν_{abs}^{p}) in a polar solvent is roughly equivalent to the difference between the steady-state emission ν_{em}^{np} and absorption frequencies ν_{abs}^{np} of the same probe in a nonpolar solvent.

$$\nu_{em}^{p}(0) \approx \nu_{abs}^{p} - \left[\nu_{abs}^{np} - \nu_{em}^{np}\right] \quad (3.7)$$

Consequently, based on the equation mentioned earlier, 3.7, one can determine the extent of solvation omitted in a picosecond configuration.

3.3 Förster Resonance Energy Transfer (FRET)

FRET occurs between two fluorophores called donor and acceptor when the molecules are sufficiently proximate, often within 1-10 nm. However, the dipole-dipole interaction via a non-radiative transition occurs when the energy of the donor is transferred to the acceptor molecule (Figure 3.3).[144]

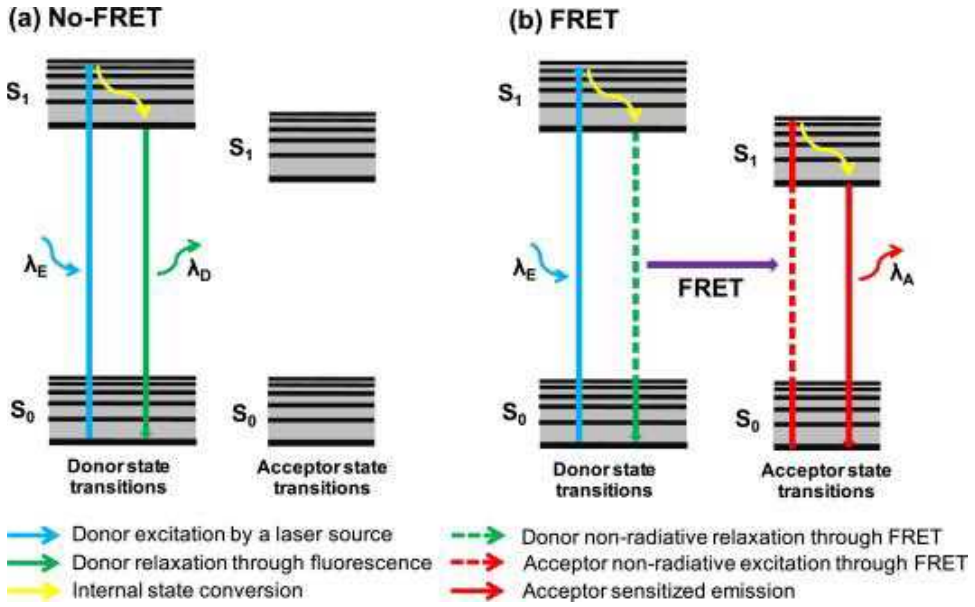


Figure 3.3 Schematic representation of FRET through Jablonski diagram. The figure is reproduced with permission from Murat Kuscu (2014).[145]

These phenomena depend upon several factors:[146]

1. The degree of spectral overlap, called overlap integral (J(λ), between the donor molecule's emission spectrum and the acceptor's absorption spectrum (Figure 3.4)

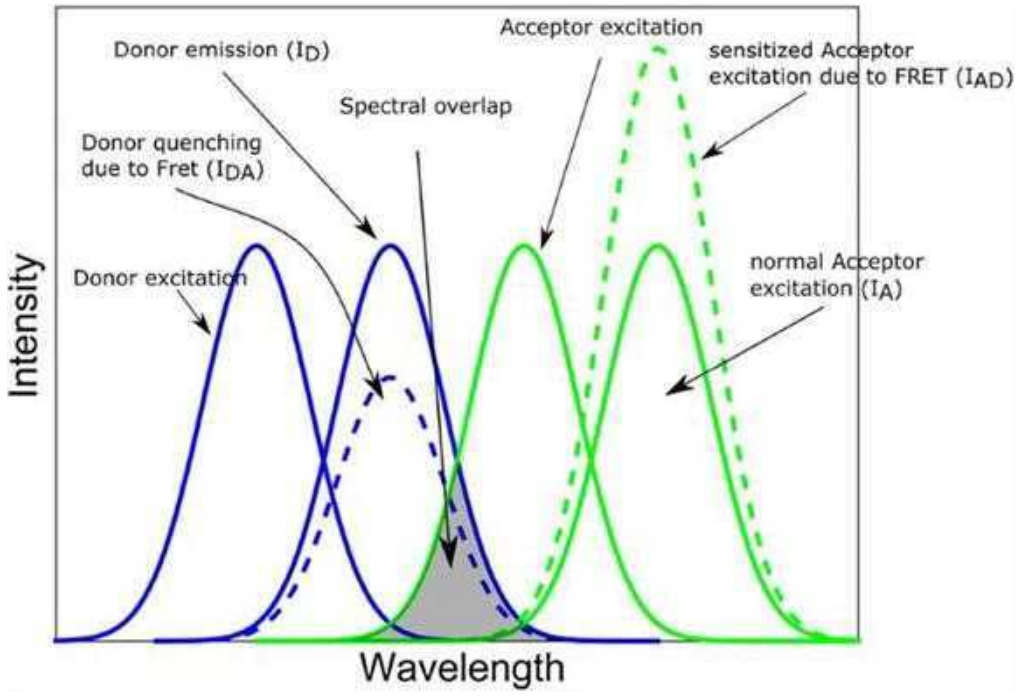


Figure 3.4 FRET spectral overlap integral (shown in grey). The figure is reproduced with permission from Georg Urstöger et al (2019).[147]

2. The relative orientation factor (κ) of the donor and acceptor transition dipoles. The range of κ^2 extends from 0 to 4. When the angle is equal to180°, κ^2 reaches its maximum value of 4; when it is parallel, κ^2 equals 1 and for orthogonal κ^2 equals 0. For freely rotating dyes, when diffusion is random, the value of κ^2 is typically considered to be 2/3.[146]
3. Quantum yield (Q_D), lifetime of the donor and reflective index (η) of the medium.

4. The E_{FRET} is highly dependent on the distance between donor and acceptor molecule, referred to as R. The specific distance when the E_{FRET} is 50 percent is referred to as the Förster distance (R_0) (equation 3.7). This distance corresponds closely to the length scale of biomolecules, such as DNA or proteins; therefore, FRET is described as a 'spectroscopic molecular ruler (Figure 3.5).

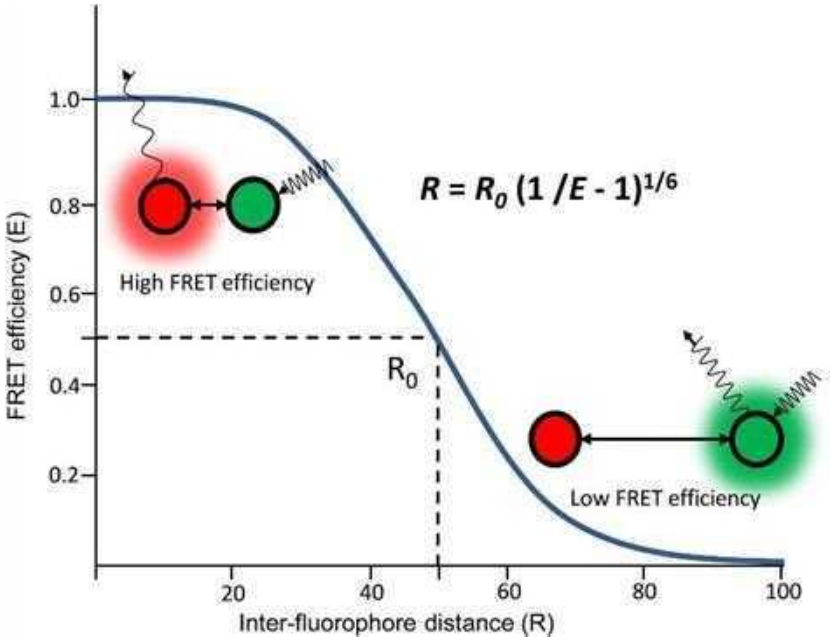


Figure 3.5 Schematic representation of how EFRET and R are dependent on each other. The figure is reproduced with permission from James D. Stephenson (2016).[148]

$$R_0 = 0.211(\kappa^2 \eta^4 Q_D J(\lambda))^{1/6} \quad (3.7)$$

The E_{FRET} can be calculated by the intensity-based (Intensity of donor I_D and acceptor I_A) method or from the distance dependent method.

$$E_{FRET} = \frac{I_A}{I_A + I_D} \quad (3.8)$$

$$E_{FRET} = \frac{1}{(1+\frac{R}{R_0})^6} \quad (3.9)$$

The most significant improvement in FRET measuring techniques is smFRET, which assesses the FRET efficiency of either a single doubly labelled molecule or a single pair of donor and acceptor-labeled molecules.[149] FRET data in bulk systems can provide significant insights; nevertheless, certain ensemble methodologies encounter challenges related to averaging, which may obscure the presence of two distinct populations in solution by presenting only their average results (Figure 3.6).[146] In smFRET allows us to see multiple single molecules with high temporal and spatial resolution to study dynamics, transitory and unidentified intermediates states.[4] TIRF is the most popular technique which is used to study smFRET, discussed in the Next section.

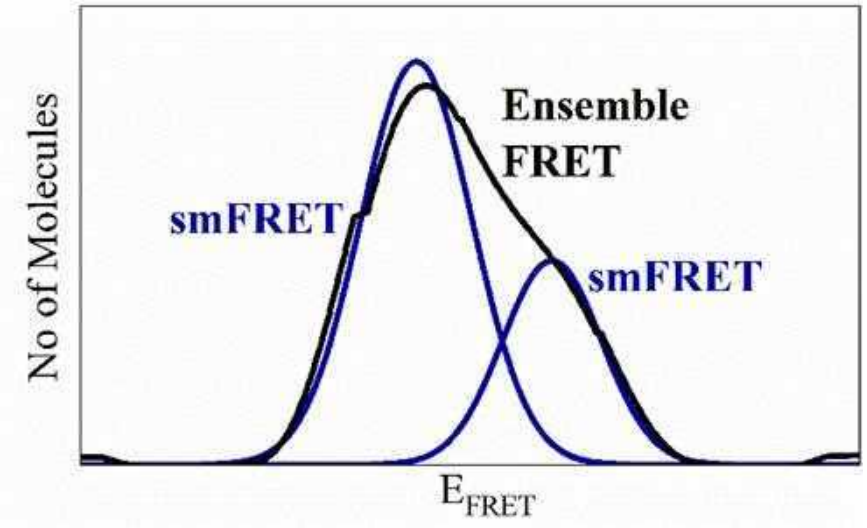


Figure 3.6 Difference Between Ensemble and smFRET.

3.4 Principle of Total Internal Reflection Microscope

TIRF is a widely used imaging technique to study single molecules.[135-136, 150-152] The concept of total internal reflection relies on an excitation light beam that travels to two different refractive index planes, and by the principle at a critical angle, the light is totally reflected, which creates an electromagnetic wave.[153] The electromagnetic wave has the same frequency as the incident light called the evanescence wave, which can penetrate a shorter distance of the sample by utilizing the phenomenon of total internal reflection to achieve high-resolution images of the molecule of interest.[135] The depth of the evanescence field can reach approximately 100 nm. It exponentially decreases as the penetration depth increases[153], depending on the wavelength of light, the angle of incidence, and the difference in the η of the medium.[135, 154] Generating the evanescent wave has the advantage of minimizing photobleaching as the illumination volume decreases while also enabling the visualization of structures below the axial diffraction limit.[155]

Researchers widely use TIRF microscopy to observe cell contacts and investigate cell adhesion, ion channels, endocytosis, and filamentous protein self-assembly. The total internal reflection microscope is also utilized to study the smFRET experiment, by which it is possible to precisely analyse the conformational change and molecular interaction of any biological system.[149, 156-160] There are two ways to develop a TIRF microscope: A) objective and B) prism-based total internal reflection microscopy. Although there are several advantages to the objective-based TIRF, e.g., the specimen here is fully accessible, and the user can easily switch between the epifluorescence mode and objective-based TIRF, which requires less complex alignment, it also has several disadvantages. Building an objective-based TIRF setup requires a higher numerical aperture objective, which can be more costly.[161-162] This objective allows confinement closer to the surface, as it focuses light at the back focal plane, so there is a possibility of light scattering within the objective, which reduces the signal-to-noise ratio.

The prism-based TIRF is the most sophisticated and cost-effective technique, providing distinct advantages, e.g., greater penetration depth as compared to objective-based TIRF.[146] It also reduces the optical abbreviation that may arise from the objective lens, which improves the spatial resolution, enhances the signal-to-noise ratio, and provides us with greater experimental flexibility by fine-tuning the excitation beam. In the prism-based TIRF, the field of illumination is higher as compared to the objective-based TIRF.[152] Here, we use a prism to attain the critical angle, directing the laser light between the glass/quartz and water media at a specific incident angle that can cause total internal reflection.[161]

Despite the numerous applications, there are currently no commercial instruments available for the prism-based TIRF microscope, which demands a substantial amount of skill to

operate such sophisticated equipment.[162-164] Here, we discussed a step-by-step guide to building the pTIFR instrument using a confocal microscope.

Table 3.1 Extensive list of microscopes and chemical's part.

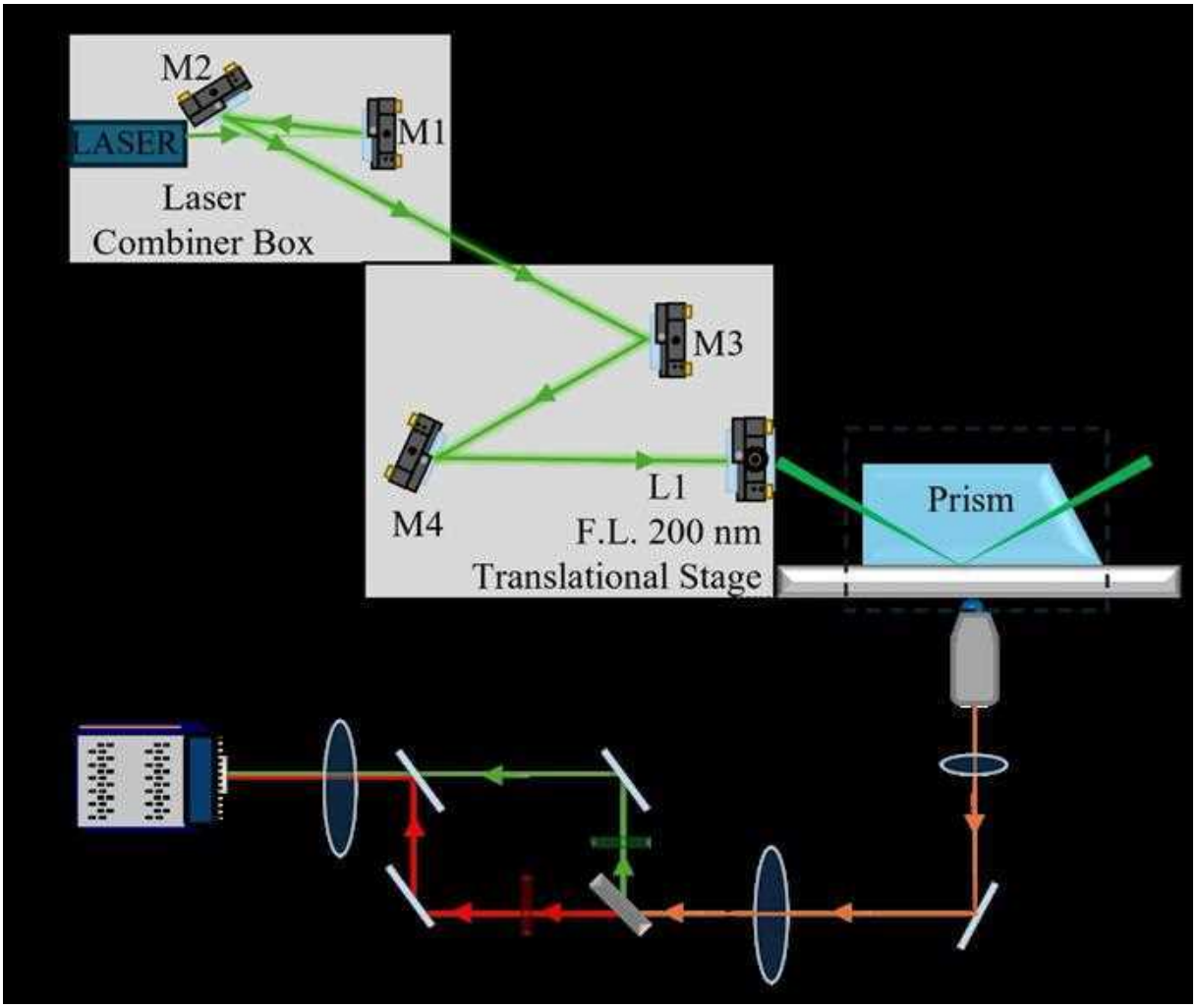
Item Description	Catalogue Number	Vendor
Standard Solid Breadboards	BB-300400-AL	Holmarc India
12 mm Diameter Posts	P-75, P-100, P-250	Holmarc India
Post Holders for 12 mm diameter Posts	PH-75, PH-100, PH-250	Holmarc India
H Type Post Base	PB-7525	Holmarc India
Square Type Post Base	PB-6550	Holmarc India
Table Clamps (L-shaped) 50x15x16 mm	L-TC-50	Holmarc India
Plano Silver Mirror	HO-PCMS-25	Holmarc India
Biconvex lens	HO-BXL25-08B	Holmarc India
Pellin Broca Prism Clear aperture = 5 mm , Material = UV Fused silica	HO-PBS-5	Holmarc India
Kinematic Mount for Circular Optics	KMC-CS-25	Holmarc India
Translation Stage	TSQ90-Mu5-03	Holmarc India
Swivel post clamp	SWPC12	Holmarc India
Right angle post clamp	RAC-12	Holmarc India
Rigid Flip Mount	FLRMM-25	Holmarc India
Right angle Post clamp	RAC-12	Holmarc India
Post Collar	PC-12	Holmarc India
Metric Socket Cap Screws	M4SHC16	Holmarc India
Metric Socket Cap Screws	M6SHC16	Holmarc India
Metric Set Screws	M4SCGB16	Holmarc India
Metric Set Screws	M6SCGB16	Holmarc India

Honeycomb Tabletop with vertical and horizontal vibration isolation		Holmarc India
Quartz Slide	42297	Alfa-Aesar
Double-sided tape Thickness (100 μM)	93010	3M
Immersion oil	56822	Sigma Aldrich
5-minute Epoxy glue		Local Vendor
Biotin BSA	9048-46-8	Sigma Aldrich
Streptavidin	434301-1MG	Thermofisher
Trolox	238813-1G	Sigma Aldrich
Glucose oxidase	9001-37-0	Sigma Aldrich
Catalase	9001-05-02	Sigma Aldrich
ssDNA		Sigma Aldrich
Laser Scanning Confocal Microscope		Olympus FV1000
EMCCD Camera with Optosplit - II		Andor iXON 897, 2021
Bandpass Filter	ET585/65m, ET706/95m	Chroma Technology
Dichroic Beamsplitters	ZT633rdc-UF2	Chroma Technology
Diamond drill bit 1.0 mm		Amazon
Black Mounting board 1mm thickness		Amazon
Electric Drilling Machine		Amazon
Tubing	0.6 mm I.D. x 1 mm O.D.	Local Vendor

3.4.1 Microscopy Setup

We developed a custom-made pTIRF setup on top of an Olympus Confocal Microscope (FV1000). First, we installed an anti-vibrational optical table with an overhead shelf to minimize table vibration and ensure proper alignment. We also chose a dark and dust-free room to minimize the noise from the stray light and the amount of dust that accumulates over time. We extracted the laser from the FV1000's laser combiner (Figure 3.7.A & 3.8). The laser combiner box, which connects to the scanner head via fibre optics during confocal imaging, consists of six lasers. We positioned a flip mirror M1 in front of the final mirror before the fibre optics, ensuring that the laser power was at its peak. To prevent dust particles, we attached black cardboard to the side of the laser combiner box, and we cut one side of the cardboard to allow the flip mirror to access

it. After the laser beam reflected through the flip mirror, it was pointed towards mirror M2, which was positioned vertically such that the beam could travel in the direction of the breadboard where M3 was located (Figure 3.7.B). The laser beam then proceeded to an elevated breadboard situated 30 cm above the optical table.



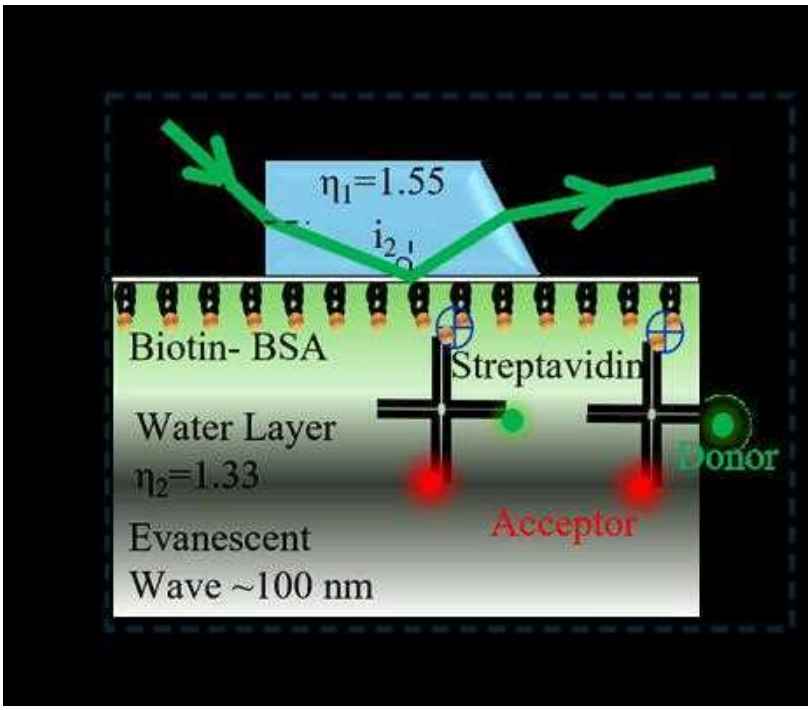


Figure 3.7 Layout of prism-based TIRF microscope. The complete system is divided into five sections: (A-B) the excitation part from the laser combiner box and at the elevated breadboard for focusing the laser beam, respectively. (C) The prism is attached to a prism holder mounted with a prism holder carried arm (discussed in Figure 3.9). In the enlarged view, we have shown the light path at the interface of the quartz/water surface, which creates almost ~100 nm evanescent wave to excite the fluorophores. (D) The emission path: The fluorescence signals are collected by a 100X oil-immersion objective with 1.45 N.A. and pass towards the optosplit. (E) Schematic representation of optosplit II. Dichroic Mirror and emission filters were used to separate the emission channel of Cy3 and Cy5 in optosplit II and projected onto the EMCCD camera.

Installation of the XYZ translation stage on the elevated breadboard takes place on the left side of the microscope and on top of the optical table (Figure 3.7.B). A distance that enables the translational stage to preserve the focusing lens's focusing distance should be using elevating the breadboard parallel to the microscope stage height. We secured the optical table with an H-type clamp to ensure stability. A custom-built prism holder carried arm, discussed in the next section, mounts the prism over the microscope stage. Precise changes to focus the laser above the objective are made possible by the 1 cm x, y, or z movement of the XYZ translational stage, to which the focusing lens was attached. To focus the laser more precisely, a plano-convex mirror with a 200 mm focal length, mounted in an XYZ translation stage, fine-tuned the laser beam to create the total internal reflection.

To position the lens, we first insert it into a lens mount (Figure 3.7.B), which also features a fine-tuning knob and a post. Then, during the translation stage, we insert it into the post holder, ensuring that the flat side faces the objective. Briefly, after receiving the laser beam from the flip mirror, the second mirror leads the laser towards the elevated platform (breadboard). We fixed two additional mirrors so that the final mirror on the breadboard focused the laser through the 200 mm lens towards the prism. We position the next two mirrors on the breadboard at approximately a 45-degree angle to focus the laser beam onto a 200-mm focal length lens. The laser path should enter the Pellin-Broca prism at the appropriate angle so that it can create the total internal reflection. We used a prism to create the total internal reflection. As a result, the incident beam can be fully internally reflected, creating an evanescent field on the quartz-water(sample) interface (Figure 3.7.C). It was essential to keep in mind to use a non-fluorescent immersion oil between the quartz slide and the prism that has the same refractive index as the slide.

For our setup, the angle of the laser beam falling on the prism was approximately 31°. At this point, it was important to control the field of view of the excitation area by placing the lens in the correct position. For the laser alignment, first focus the 0.1 μm fluorescence bead on the flow chamber (discussed in the next section) to fix the objective height using the epifluorescence light. Once you can see the sample through the eyepiece, proceed to align the laser. Next, aim the laser at the top of the objective, ensuring it is roughly focused. After this, apply a small drop of non- immersion oil to the top of the sample chamber and position a prism with a prism holder carried arm on top of it.

To achieve this, we secure the first prism holder carried arm on the microscope body and loosen the prism holder's (the technical details are described in Figure 3.9) screw to adjust the prism position during the alignment process easily. Next, we place the prism on top of the sample chamber, ensuring that it remains flat against the sample chamber. After that, we performed a rough alignment to reflect the laser beam from the prism, ensuring that the field of view was centred in the lower objective through the eyepiece. With the completion of the alignment, we tighten the prism holder screw to secure the prism with the adapter. Fixing the prism to the microscope body was crucial to prevent the excitation beam from moving when the sample moved in the x-y direction to collect images in different areas. Following this, we primarily utilized the transitional stage for fine alignment each time we swap out the sample. Every time we experiment with a new sample chamber, we must first remove the prism adapter to position

the sample chamber above the objective, necessitating a fine alignment. To capture the image, we currently use the EMCCD camera and the micromanager software. Next, we utilize the translation stage to align the Z-axis, ensuring the bead sample reaches its maximum intensity.

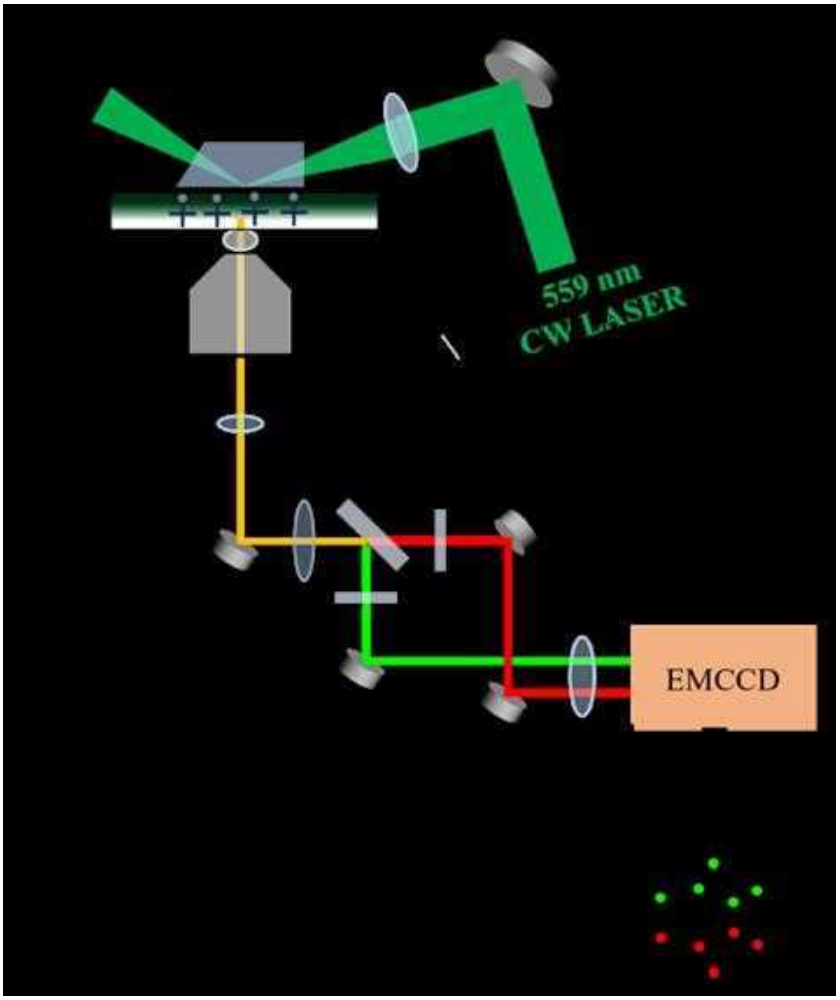


Figure 3.8 Optical setup of pTIRF microscope to study smFRET. Laser is directed through a biconvex lens (L1) of 200 mm focal length on a prism to create an evanescent field at the interface of quartz and water. The fluorescence signals from a sample are collected by a 100X oil-immersion objective with 1.45 NA and passed through a 1X tube lens (TL) toward the detector for recording. D (green) and A (red) signals are separated by a dichroic mirror (DM, Chroma: ZT633rdc-UF2) and then pass through bandpass filters (BP) - ET585/65m for donor and ET706/95m for acceptor channels. Then, both signal channels are passed through the L3 lens which focuses signals at the EMCCD camera in side-by-side orientation. The focal length of L2 and L3 is the same, and the combination of them makes a 4f relay system to move the image plane.

3.4.2 Calculation of Critical Angle and the Depth of Penetration.

We have also calculated the incident laser beam angle for the total internal reflection. According to Snell's law[154-155, 162-163]

$$\eta_1 \sin\theta_1 = \eta_2 \sin\theta_2 \qquad (3.10)$$

Where the incident beam and refracted beam are represented by θ_1 and θ_2 respectively, at the glass/water interface, and the refractive indices of medium 1 (glass surface= 1.55) and medium 2 (water = 1.33) are represented as η_1 and η_2, respectively. The quartz/water surface's critical angle is

$$\theta_c = \sin^{-1}\frac{\eta_2}{\eta_1} = \sin^{-1}\frac{1.33}{1.55} = 59.1° \quad (3.11)$$

Therefore, in accordance with Snell's law, the i_2, as shown in Figure 3.7.C, must equal or exceed 59.1 in order to produce a total internal reflection. For our setup, the angle of the laser beam falling on the prism was i_1~31°. So, as per the calculation, the i_2 was approximately 71°, which was greater than the critical angle of the glass/water surface. We have also calculated the depth of penetration using the equation.[155, 163]

$$d = \frac{\lambda}{4\pi}(\eta_1^2 \sin i_2 - \eta_2^2)^{1/2} \quad (3.12)$$

As the λ is the incident light's wavelength (for our case, 559 nm), the depth of penetration was approximately 73 nm. However, the incident angle and the medium's refractive index have a significant impact on the penetration depth.

3.4.3 Prism Holder and Prism Holder Carried Arm

A holding device (Figure 3.9.C) with a prism-carrying arm (Figure 3.9.A) mounted to the top part of the microscope was used to secure the prism above the flow cell. We have used aluminium machining to create our custom prism holder, and holder carried arm. The holder carried the arm's measurements, and the prism's height will vary depending on the microscope. Still, the design's primary idea—fixing the prism's location directly over the objective remains constant. We internally created our prism holder and prism holder carried arm, as shown in Figure 3.9. The prism we tightened the Prism (Pellin-Broca, 11 mm x 20 mm x 6.4 mm) to the holder using M4 screws, keeping in mind that the holder size only accommodates a specific prism; for other prism sizes, we need to modify the design slightly. We have mounted the prism holder onto the holder carried arm with a post as per Figure 3.9 and used a right-angle post clamp and post collar to fix it. Although the prism holder and prism holder carried an arm designed for our setup, readers may utilize it as per their setup. In our scenario, we affixed the 20 mm post holder to the IX81 microscope body using an M4 screw, followed by the attachment of the prism holder carried arm; (Figure 3.9 details all the dimensions. We determine the precise location for the screw head to fix the holder based on the dimensions of the setup and the location of the prism that we must mount to achieve TIR.

3.4.4 Emission Path

We collected the fluorescence emission using the confocal microscope's transmission mode. We collected and separated the emission data from the excited fluorophore using the Optosplit II. First, we collected the emission from the 1.45 N.A. 100X objective to a tube lens (1X) in the FV1000, and then used the mirror (M5) to reflect it towards the optosplit. A C-mount adapter connects the optosplit to the left port of the FV1000. A filter cube made up of the dichroic mirror D.M. (chroma: ZT633rdc-UF2) is inserted by the optosplit. This separates the donor and acceptor signals before they go through the bandpass filters (B.P.): ET585/65m for the donor channels and ET706/95m for the acceptor channels. The focal lengths of L2 and L3 were the same, creating a 4F relay system for clear transmission of the microscope image. We connect the optosplit electron-multiplying charge-coupled device to the exit port and mount it on the optical table. The data collection software allows us to rotate the camera image either anticlockwise or clockwise. We primarily used Micromanager[165] software to record the video in .tiff format and

then processed the data using SPARTAN software.[166] The manufacturer may provide detailed information about the camera manual or the data processing and collection software manual.

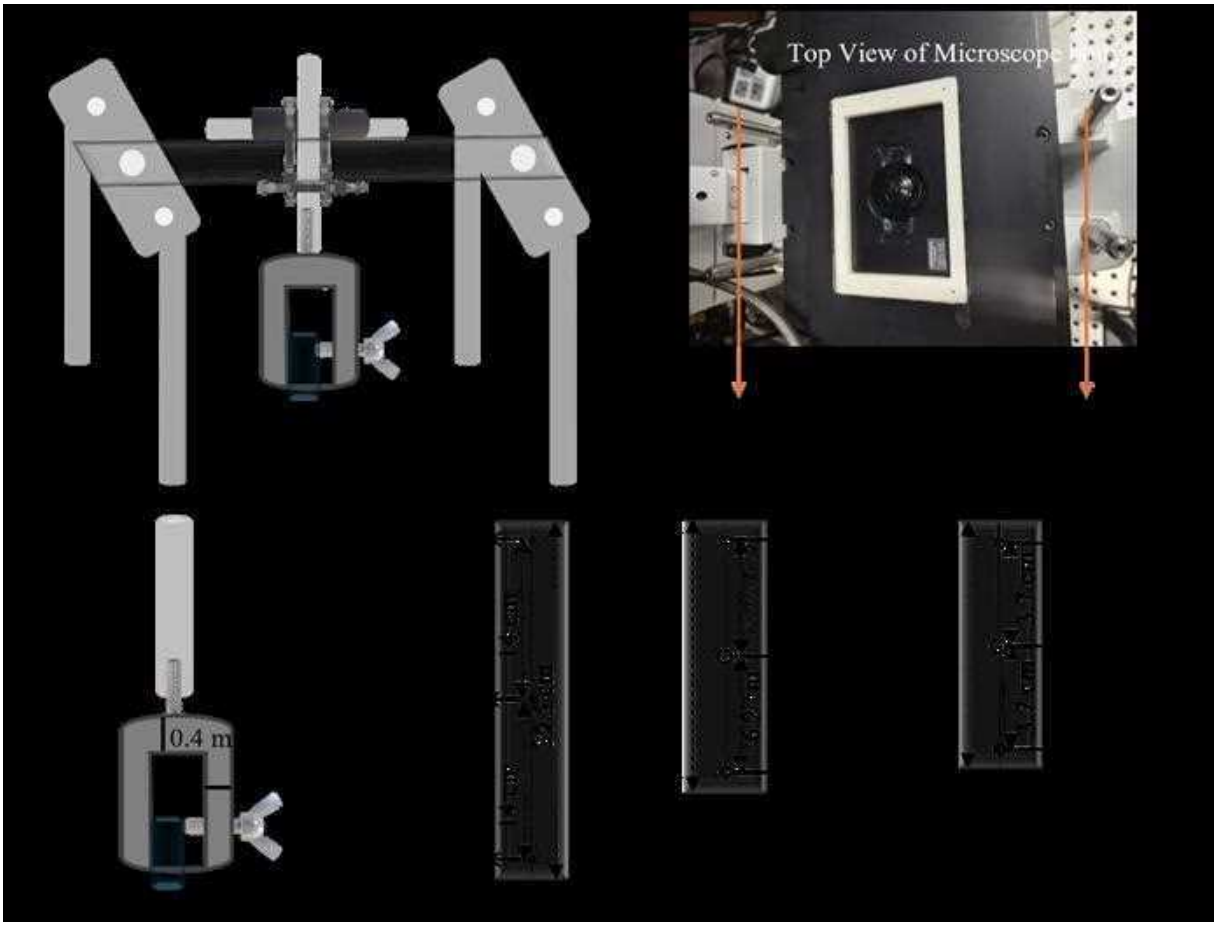


Figure 3.9 Schematic representation of prism holder and prism holder carried arm. (A) The dimension of the prism holder carried arm which consist of 3 aluminium plates as shown in a1, a2 and a3. (B) Real image of the top view of the microscope body used to hold the prism holder carried arm. (C) The dimension and layout of the prism holder.

3.4.5 Sample Chamber Preparation

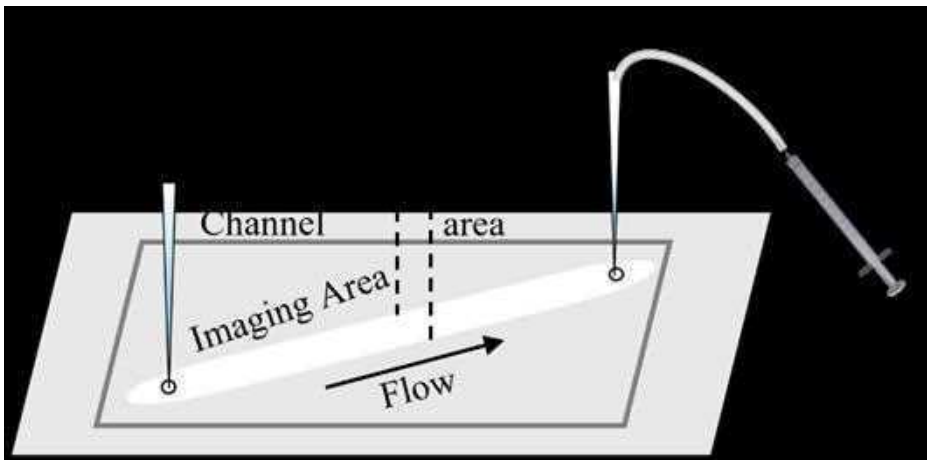


Figure 3.10 Schematic representation of sample chamber. The two corners of the quartz slide were drilled with the help of a diamond drill bit. Using double-sided tape (thickness 100 µM) as a spacer, a sandwich construction comprising the cover slide and cover glass was used to build the sample chamber. The two sides hole was then attached with a 200 µl pipette tip using the help of 5 minutes of epoxy resin. A pipette was used to flow the channel, and a 1 ml syringe was used to create suction in the outlet area. The arrow shows the flow direction of the sample.

We made sample chambers using a sandwich assembly of quartz slide and cover glass and sealed them with double-sided tape. The procedure is described below. [167]

1. Take a quartz slide (76.2 × 25.4 × 1.00 mm) and create two diagonal holes by using the diamond drill bit of 1 mm.
2. After creating the hole, thoroughly clean the slide as described in the cleaning procedure.
3. Cut the double-sided tape diagonally (of approximately ~ 5 mm widths) in the middle, as described in Figure 3.10.
4. Place one side of the double-sided tape on the slide and cover the other side with the coverslip to create a sample chamber of around 30-40 µl. To seal the chamber and remove any air bubbles properly, gently press the coverslip.
5. Cut 200 µl tips that are approximately 1 mm long. Next, place 200 µl of the pipette tip into each of the quartz slide's two holes. This establishes a route for the exchange of solutions at the inlet and output. Finally, seal the parts with 5 minutes of epoxy glue.
6. On the inlet side, use a pipette to insert the sample, and on the other side, attach a tube of (0.6 mm inner diameter x 1 mm outer diameter) to create suction with a 1 ml syringe.
7. Carefully inject the sample to ensure that no air bubbles enter the chamber.
8. After using the sample chamber, place it in water for at least 12 hours to remove the double-sided tape, and you can reuse the quartz slide.

3.4.6 Cleaning Procedure

1. Boil the slide in MiliQ water for approximately 10 minutes.
2. Sonicate the slide in 0.1N NaOH for 15 minutes, NaOH is important to remove any biological residue.
3. Wash with tap water by gently scrubbing the slide.
4. For 15 minutes, sonicate the slide in acetone to get rid of any organic residue, followed by washing with Milli Q water.

3.4.7 KOH Etching Procedure

1. The slide and coverslip were both sonicated in 1M KOH solution for 20 minutes.
2. The slide and coverslip were both rinsed and sonicated with MiliQ water for 15 minutes.
3. Sonicate 20-30 minutes again the slide in 1M KOH and wash with water to make the surface hydrophilic.
4. Dry the coverslip and slide with N_2 gas to avoid any water spots in the slide, and burn the slide with a propane torch for 2 minutes to burn any leftover fluorescent residue.
5. Burn the coverslip with a propane torch for 20-30 seconds only; it may break if it burns for too long.

3.4.8 DNA HJ Preparation

We purchased all the modified and unmodified ssDNA from Sigma Aldrich (custom-made) and used it without further purification. The sequence of four single-strand DNAs is given as follows:

Cy5 labelled	5′-Cy5-CCC TAG CAA GCC GCT GCT ACG G-3′
Cy3 labelled	5′-Cy3-CCG TAG CAG CGC GAG CGG TGG G-3′
Biotin labelled	5′-Biot-CCC ACC GCT CGG CTC AAC TGG G-3′
Unlabelled	5′-CCC AGT TGA GCG CTT GCT AGG G-3′

We prepared the DNA HJ by thermally annealing the ssDNA at a concentration of 2.5 μM in annealing buffer (10 mM tris HCl at pH=8.0, 50 mM NaCl, and 15 mM $MgCl_2$,6H_2O).[124] We determined the cy3:cy5:biotin: unlabeled ratio to be 1:2:1:2. We carried out the annealing process by lowering the solution's temperature from 96°C to 4°C at 0.5°C /min in a thermal cycler. We stored the assembled junction at 4°C for future use.

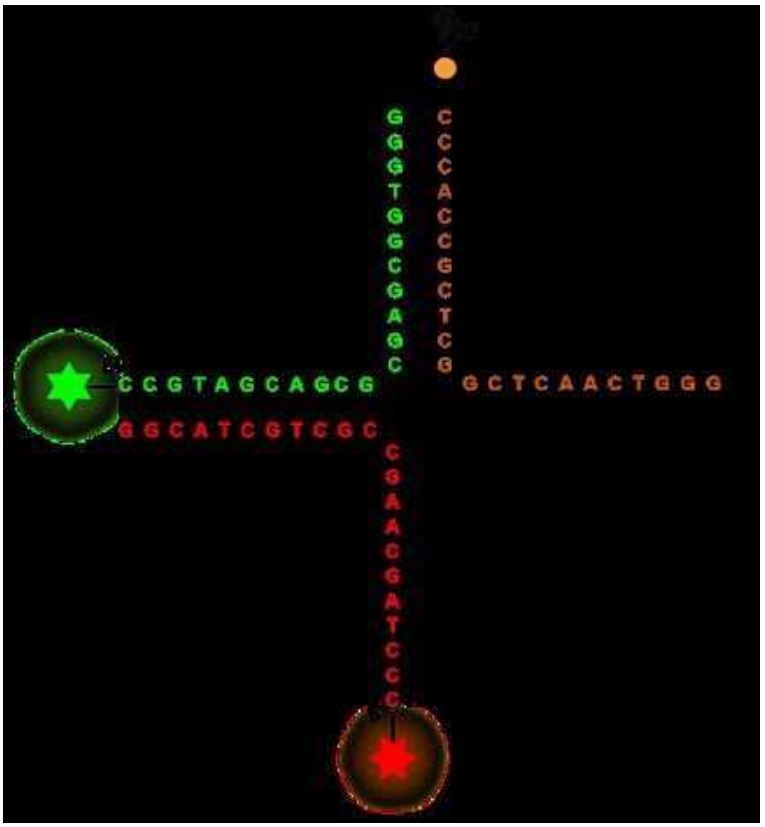


Figure 3.11 The sequence of four DNA oligos to form the DNA Holliday Junction.

3.4.9 Preparation of Oxygen Scavenger Solution (Trolox)

Excited singlet and triplet states are generally more reactive than the ground electronic state. Initially, electron cloud polarization is more probable in an excited molecule due to the promoted electron's increased distance from the nucleus. An increased propensity for polarization enhances a molecule's reactivity. Secondly, absorbed resonance energy diminishes the activation energy required to facilitate photochemical processes. Comparing the reactivity of excited singlet and triplet states reveals that the triplet state is typically more reactive. The slow rate of phosphorescence allows internal conversion and other non-radiative mechanisms to compete with the radiative relaxation of the triplet state effectively. The probability of reactive intermediates is consequently greater than that of the excited singlet state, where the rapid fluorescence depletion of the excited singlet state more efficiently competes with the chemical pathways that yield such intermediates. In both instances, a portion of the intermediates undergoes photobleaching, an irreversible reaction that significantly alters a molecule's absorption and emission properties, leading to a permanent loss of fluorescence. Keep in mind

that triplet quenching and intersystem crossover were facilitated by molecular oxygen. A highly reactive higher energy singlet oxygen is a byproduct of the role of molecular oxygen. The molecule loses an electron to oxidation during the reaction, which also causes it to lose its fluorescence. Without an oxygen scavenging mechanism, the dyes Cy3 and Cy5 are photostable for a short amount of time. The lifespan of the dye is extended by the inclusion of an enzyme oxygen scavenging mechanism. A combination of enzymes that includes glucose oxidase, catalase, and glucose improves the lifetime of the fluorescent dyes by efficiently removing oxygen. However since oxygen is a particularly effective triplet state quencher, removing oxygen increases the lifetime in the triplet state. Thus, many photo-blinking events occur in the single molecule time traces as a result of the introduction of an oxygen scavenging system. Reducing agents are particularly effective in preventing photoblinking events. For instance, Trolox at concentrations between 1 and 5 mM is said to be a particularly powerful triplet state quencher, as is beta-mercaptoethanol (β-ME), an analogue of vitamin E.

For all our experiments, Trolox (30 mg) was dissolved in water (5 ml) using vortex; we were able to create the stock solution of (~4 mM) Trolox. To achieve better solubility, we added 1 M NaOH drop by drop to the solution. After mixing, to estimate the exact concentration, we used a 0.2-µm syringe filter to filter the solution. Then, we examined the absorption spectra at 290 nm (with an extinction coefficient of 2350 ± 100 M^{-1} cm^{-1}). Trolox is utilized as a triplet-state quencher to increase the dye's photostability.

3.4.10 Preparation of Imaging Buffer (T50) Solution

T50 buffer is a mixture of 10 mM Tris-HCl and 50 mM NaCl at pH 8.0. For the Imaging Buffer preparation to avoid any impurities, we prepared 0.2 mg/ml stock catalase solution in T50 buffer. Based on this, we combined 10 mg of glucose oxidase with 20 µl of 0.2 mg/ml catalase in 80 µl of T50 buffer. In order to mix the ingredients, we centrifuge at a higher speed for one minute, extract the supernatant, and store it at 4 ^{o}C. In this way, 100X gloxy solution was prepared. We prepared 0.8 % w/v D-glucose in the T50 buffer. We added Trolox and gloxy solution in such a way that the final solution of the imaging buffer contains 2 mM of Trolox solution and 1X gloxy. Just before the measurement, with the minimal amount of air exposure possible, we must add glucose to the glucose-containing buffer.

3.4.11 Immobilization Techniques

To immobilize the biotinylated DNA HJ to the quartz slide, 30 µl 1 mg/ml of Biotin BSA was pipetted into the sample chamber. It was suctioned to the chamber with the help of a syringe. After 5 minutes, it was flushed with 100 µl of T50 buffer at least three times. Then again, using the same procedure, 0.2 mg/ml streptavidin was introduced, and after 1 minute, it was flushed with 100 µl of T50 three times to ensure the removal of any nonspecific binding. After that, we added biotinylated DNA, waited for 3 minutes, and the sample was flushed with 200 µl imaging buffer to eliminate freely moving molecules. We generally used 100-200 pM DNA HJ solution for our experiment, although it highly depends on the setup, the optimal number of molecules, and other things. After the laser has been aligned with a standard bead sample, adjust the field of view by positioning the sample chamber on the stage adapter.